Magnetostatic modes of lateral-magnetic-superlattice films in a transverse field

1997 J. Phys.: Condens. Matter 9 5777

(http://iopscience.iop.org/0953-8984/9/27/009)

J. Phys.: Condens. Matter **9** (1997) 5777–5786. Printed in the UK PII: S0953-8984(97)78502-3

Magnetostatic modes of lateral-magnetic-superlattice films in a transverse field

Xuan-Zhang Wang†‡ and D R Tilley§‖¶

† China Centre of Advanced Science and Technology (World Laboratory), PO Box 8730, Beijing 100080, People's Republic of China

‡ Department of Physics, Harbin Normal University, Harbin 150080, People's Republic of China

§ School of Physics, Universiti Sains Malaysia, 11800USM Penang, Malaysia

‖ Department of Physics, University of Essex, Colchester CO4 3SQ, UK

Received 9 October 1996

Abstract. We discuss some properties of magnetostatic modes of a lateral superlattice (LSL) consisting of a ferromagnetic film patterned into a series of parallel stripes. In contrast to earlier work we assume that the applied magnetic field and static magnetization are transverse to the stripes. The details of the results depend on f_1, the fraction of the patterned film occupied by magnetic material. We find a surface mode for all values of f_1, propagating in a wedge centred about the Voigt direction. In a thick (semi-infinite) LSL the surface mode lies above the bulk continuum and for an LSL of finite thickness the bulk continuum is replaced by a spectrum of discrete guided modes.

1. Introduction

Among the magnetic low-dimensional structures that are the subject of extensive investigation, lateral superlattices (LSLs) are attracting considerable interest. Fabrication [1–4] is by lithographic patterning of a magnetic film to produce a structure of the kind illustrated in figure 1. Although the experimental problems in producing high-quality samples are considerable, it seems to us timely to try to develop a general theoretical understanding of the possible excitation modes of LSLs. The various regimes that may be found can be anticipated from experience with magnetic thin films and multilayers [5]. Potentially one of the most important sorts of excitation in a ferromagnetic LSL are pure magnetostatic modes with Bloch wavevector K satisfying $KD \ll 1$ since these should be accessible to Brillouin scattering [5]. When this inequality holds the LSL should be described by the effective-medium approximation, which has been applied extensively in far-infrared spectroscopy of semiconductor superlattices [6] and in magnetic superlattices [7]. We have used this method for the magnetostatic modes on the surface of a thick ferromagnetic LSL [8] and more recently for the magnetostatic surface-type and guided modes of a ferromagnetic LSL of finite thickness [9]. Subsequently we dealt with an antiferromagnetic LSL [10], also within the effective-medium approximation; in this case it is necessary to include the effects of retardation because far-infrared spectroscopy, which is the only established experimental technique [7, 11–13], probes the region $K \approx \omega/c$. In [8–10] we assumed that the magnetic field and the ordering direction were parallel to the

¶ Corresponding author: D R Tilley, School of Physics, Universiti Sains Malaysia, 11800 USM Penang, Malaysia. E-mail address: david@usm.my

0953-8984/97/275777+10$19.50

LSL grooves, i.e. along the X axis in figure 1. One set of results is that in simple cases, the ferromagnet and the antiferromagnet without applied field, the surface mode is found only for magnetic fraction $f_1 = d_1/D > 0.5$. In the presence of a magnetic field the retarded modes of the antiferromagnetic LSL change their character from real to virtual as f_1 drops through 0.5. Similar results were already known [14–16] for conventional superlattices.

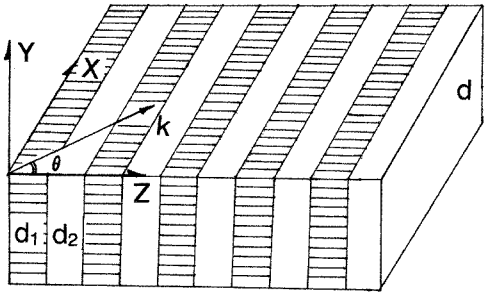

Figure 1. A lateral magnetic superlattice. Magnetic lines of width d_1 are separated by non-magnetic spacers of width d_2 so that the superlattice period is $D = d_1 + d_2$. The structure has depth d. Axes are defined as shown and a static field H_0 is applied normal to the layers, along Z. We discuss propagation of surface and guided magnetostatic modes in the direction defined by the angle θ.

In a subsequent paper [17] we considered a regime of larger wavenumbers K in which exchange effects would become significant and the relevant excitations are dipole-exchange modes, which in some cases are of importance in Brillouin scattering from ferromagnetic films [5]. We discussed there the modes of an isolated rectangular magnetic wire which is a simple model of one of the stripes in figure 1.

In the present paper we return to the purely dipolar modes described within the effective-medium approximation. Camley *et al* [18] have recently addressed the important spectroscopic problem of extracting magnetic features from the spectra of metallic samples in which there is usually a high background reflectivity. They were led to consider a LSL in which the external field, the ordering direction and most importantly the E field of the incident wave are perpendicular to the grooves. The effective conductivity in the E direction is then small and according to their calculations the background reflectivity is reduced and the magnetic features become visible. This work has drawn attention to geometries of this kind and we think it worthwhile to carry out related calculations of magnetostatic or retarded modes.

The configuration and axes to be used are defined in figure 1. We discuss the magnetostatic modes of a ferromagnetic LSL with H_0 and M_0 along Z; we deal with both a 'thick' (large-d) LSL and with the general case. As stated, we employ the effective-medium approximation. The conditions for validity can be seen from the first discussions of magnetic superlattices [19, 20] as well as from the earlier work on optical superlattices [21, 22]. One requirement, as mentioned, is that the Bloch wavelength $2\pi/K$ in the Z direction should be long compared to the period D, and this is automatically satisfied for magnetostatic modes. It is further necessary that the wavelength within each layer should be large compared with the layer thickness d_1. This may be satisfied provided that the magnetic boundary conditions at the interfaces are that the spins are unpinned. For pinned spins the boundary condition on the rf magnetization $\boldsymbol{m}$ is $\boldsymbol{m} = 0$ [23] so that within each layer $\boldsymbol{m}$ has a standing-wave profile and the condition of slow variation is not met. The

assumption underlying this work is therefore that the boundary conditions correspond to unpinned spins.

2. The permeability tensor

The permeability tensor $\boldsymbol{\mu}(\omega)$ within each ferromagnetic layer is given by the usual expression [24] except that the demagnetization factor is unity and therefore the resonance frequency is

$$\omega_i = \gamma H_{\mathrm{i}} = \gamma(H_0 - 4\pi M_0) = \omega_0 - \omega_m \tag{1}$$

in conventional notation. Thus

$$\boldsymbol{\mu}(\omega) = \begin{pmatrix} \mu & \mathrm{i}\mu_\perp & 0 \\ -\mathrm{i}\mu_\perp & \mu & 0 \\ 0 & 0 & 1 \end{pmatrix} \tag{2}$$

with

$$\mu = 1 + \omega_m\omega_i/(\omega_i^2 - \omega^2) \tag{3}$$

$$\mu_\perp = \omega_m\omega/(\omega_i^2 - \omega^2). \tag{4}$$

The appearance of the internal field H_{i} in (1) means that the properties of the modes that we shall discuss are different from those of a continuous film even for small non-magnetic fraction f_2. With H_0 parallel to the layers we find [8] that as $f2 \to 0$ the standard results for the Damon–Eshbach modes are recovered. In the present case, however, the existence of non-magnetic gaps, however small, means that the resonance frequency is always determined by H_{i} rather than H_0.

The effective-medium permeability $\boldsymbol{\mu}^{eff}(\omega)$ may be derived by the usual field-continuity method [19, 21], which in the present case means continuity of h_x and h_y at the interfaces. We find

$$\boldsymbol{\mu}^{eff}(\omega) = \begin{pmatrix} \mu_{xx} & \mathrm{i}\mu_{xy} & 0 \\ -\mathrm{i}\mu_{xy} & \mu_{yy} & 0 \\ 0 & 0 & 1 \end{pmatrix} \tag{5}$$

with

$$\mu_{xx} = \mu_{yy} = f_1\mu + f_2 \tag{6}$$

$$\mu_{xy} = f_1\mu_\perp \tag{7}$$

where $f_i = d_i/D$ so that f_1 and f_2 are the fractions of magnetic and non-magnetic material.

3. The surface magnetostatic mode on a thick LSL

We consider first the case of large d so that the LSL is treated as semi-infinite. The derivation of the surface-mode dispersion relation is standard [24] and we review it only briefly. Since $\boldsymbol{\nabla} \times \boldsymbol{h} = 0$ we introduce a scalar potential ψ so that $\boldsymbol{h} = \nabla\psi$ and for the propagation direction shown in figure 1 we take

$$\psi = A_0 \exp(\mathrm{i}\boldsymbol{k}\cdot\boldsymbol{r} - \alpha_0 y)\exp(-\mathrm{i}\omega t) \qquad y > 0 \tag{8}$$

$$\psi = A_1 \exp(\mathrm{i}\boldsymbol{k}\cdot\boldsymbol{r} + \alpha y)\exp(-\mathrm{i}\omega t) \qquad y < 0. \tag{9}$$

Here $\boldsymbol{k}$ and $\boldsymbol{r}$ are two-dimensional vectors in the X–Z plane. The relations $\boldsymbol{b} = \boldsymbol{\mu}^{eff}\boldsymbol{h}$ and $\boldsymbol{\nabla}\cdot\boldsymbol{b} = 0$ lead to

$$a_0^2 = k^2 \tag{10}$$

and

$$\mu_{xx}(k_x^2 - \alpha^2) + k_z^2 = 0. \tag{11}$$

The boundary conditions ψ and b_y continuous at $y = 0$ lead to two relations between A_0 and A_1 and consistency between these gives the dispersion relation in the implicit form

$$\alpha_0 + \mu_{xy}k_x + \mu_{xx}\alpha = 0 \tag{12}$$

which with use of (10) and (11) may be reduced to

$$(1 + \mu_{xy}\sin\theta)^2 = \mu_{xx}(\mu_{xx}\sin^2\theta + \cos^2\theta). \tag{13}$$

With use of (3), (4), (6) and (7) we can finally write (13) in the explicit form

$$\omega = [\omega_0 - \omega_m + \sin^2\theta(\omega_0 - f_2\omega_m)]/2\sin\theta. \tag{14}$$

For the solution of (12), (13) or (14) to represent a surface mode the additional conditions $\alpha > 0$ and $\alpha_0 > 0$ must be satisfied.

We find that like other surface magnetostatic waves these modes propagate only in a range of angles $\theta_c < \theta < \pi - \theta_c$ centred on the positive X axis. At the critical angle $\alpha = 0$ (infinite penetration depth), so as seen from (10) and (12) $1 + \mu_{xy}\sin\theta_c = 0$ and it follows from (13) that

$$\mu_{xx}(\mu_{xx}\sin^2\theta_c + \cos^2\theta_c) = 0. \tag{15}$$

The second factor in (15) does not vanish for any real value of θ. From $\mu_{xx} = 0$ it follows that the mode frequency ω_c for $\theta = \theta_c$ is given by

$$\omega_c^2 = (\omega_0 - \omega_m)^2 + f_1\omega_m(\omega_0 - \omega_m) \tag{16}$$

and substitution in (14) then gives

$$\sin^2\theta_c = (\omega_0 - \omega_m)/(\omega_0 - f_2\omega_m). \tag{17}$$

This equation has some rather surprising properties. First, for $\omega_0 > \omega_m$ there is a solution for θ_c and therefore a surface mode is found for all values of f_2 but only in a restricted wedge of angles of propagation. For $\omega_0 < \omega_m$ on the other hand (17) has no solution for real θ_c for any value of f_2. Thus there is no magnetostatic mode for any angle of propagation for $\omega_0 < \omega_m$. As seen from (1) the condition $\omega_0 > \omega_m$ means that the external field H_0 is sufficiently large that the internal field H_i within each magnetic layer is in the same direction as H_0.

As mentioned, the fact that a mode exists for all values of $f_2 = 1 - f_1$ is unusual. For the LSL with H_0 parallel to the layers we found [8] that the surface mode exists only for $f_1 > 0.5$, that is, when the magnetic fraction is larger than the non-magnetic fraction. This is similar to the well known result [14, 15] that there is no magnetostatic mode on a conventional magnetic superlattice for $f_1 < 0.5$. The dependence of θ_c on f_2 is illustrated in figure 2.

The results of this section are illustrated further in figure 3, where we show examples of the variation of mode frequency ω with angle θ for two values of f_1 and $H_0 = 7.032$ kG ($\omega_0/\omega_m = 1.166$) for a Ni–non-magnet LSL. On these graphs we show also the bulk-mode continuum. The boundary curves of this are found from (11) first by putting a $\alpha = 0$ (bulk mode propagating parallel to surface) and second by putting $k_x = k_z = 0$ and $\alpha = \mathrm{i}k_y$ (bulk mode propagating normal to surface). The first operation gives for the lower limiting frequency

$$\omega = \omega_l = [(\omega_0 - \omega_m)^2 + f_1\sin^2\theta\,\omega_m(\omega_0 - \omega_m)]^{1/2} \tag{18}$$

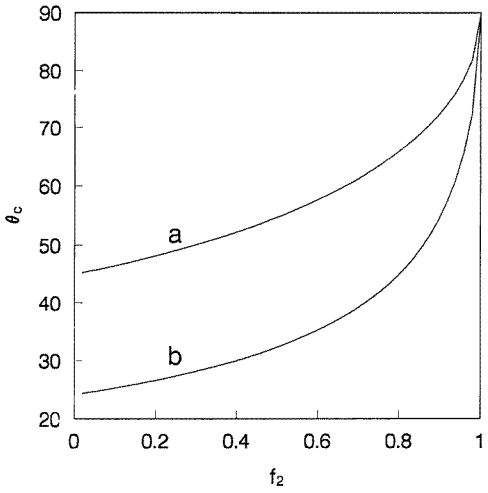

Figure 2. Dependence of critical angle θ_c on non-magnetic fraction f_2 for $\omega_0/\omega_m = 2.0$ (curve a) and $\omega_0/\omega_m = 1.2$ (curve b).

and the second gives the upper limiting frequency as $\omega = \omega_c$, where ω_c was previously defined in (16) as the surface-mode frequency at the critical angle θ_c. Thus (16) implies that at the critical angle the surface mode merges with the top of the bulk continuum as indeed is seen in figure 3.

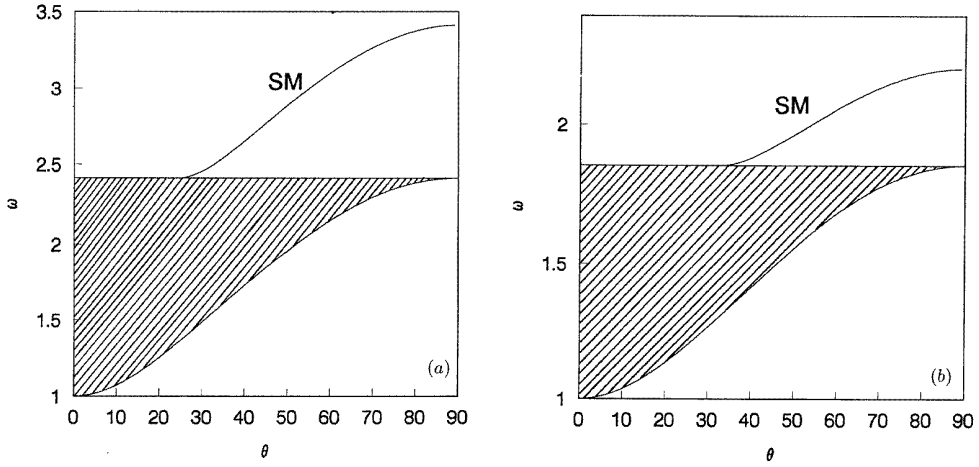

Figure 3. Surface-mode frequency versus θ for a magnet–non-magnet LSL in external field $H_0 = 7.032$ kG and magnetic fraction f_1 equal to (a) 0.8 and (b) 0.4. The magnetic material is Ni with $4\pi M_0 = 6.032$ kG. The surface mode is denoted by SM and the bulk continuum defined by (18) and (19) is shown shaded.

4. General thickness: surface and guided modes

We now turn to the case where the depth d in figure 1 has a general value. The potential now takes the form

$$\psi = A_0 \exp(\mathrm{i}\boldsymbol{k}\cdot\boldsymbol{r} - \alpha_0 y)\exp(-\mathrm{i}\omega t) \qquad y > 0 \tag{19}$$

$$\psi = \exp(\mathrm{i}\boldsymbol{k}\cdot\boldsymbol{r})[a\exp(\alpha y) + b\exp(-\alpha y)]\exp(-\mathrm{i}\omega t) \qquad 0 > y > -d \tag{20}$$

$$\psi = A_1 \exp(\mathrm{i}\boldsymbol{k}\cdot\boldsymbol{r} + \alpha_0 y)\exp(-\mathrm{i}\omega t) \qquad y < -d. \tag{21}$$

Formally, α_0 and α are still given by (10) and (11) but now α can take imaginary values, corresponding to guided modes, as well as real values, corresponding to modified surface modes. The calculation now follows the standard form [24]. The boundary conditions of constant ψ and b_y at $y = 0$ and $-d$ give four homogeneous equations in the four amplitudes A_0, a, b and A_1 and the condition for consistency gives the dispersion equation. This is

$$(\alpha_0^2 - \mu_{xy}^2 k_x^2 + \mu_{xx}^2\alpha^2)\tanh(\alpha d) + 2\alpha_0\alpha\mu_{xx} = 0 \tag{22}$$

and with use of (10) and (11) this may be written

$$[1 + (\mu_{xx}^2 - \mu_{xy}^2)\sin^2\theta + \mu_{xx}\cos^2\theta]\tanh(\Lambda k d) + 2\Lambda\mu_{xx} = 0 \tag{23}$$

where we have defined $\alpha = \Lambda k$ so that

$$\Lambda = [(\mu_{xx}\sin^2\theta + \cos^2\theta)/\mu_{xx}]^{1/2}. \tag{24}$$

For real α (23) describes how the surface modes of the previous section are modified by the presence of a second surface. It applies also for imaginary α in which case it describes how the bulk continuum is broken up into a discrete guided-wave spectrum in the film of finite depth. It is convenient to write the guided-wave dispersion equation in the explicit form

$$[1 - (\mu_{xx}^2 + \mu_{xy}^2)\sin^2\theta - \mu_{xx}\cos^2\theta]\tan(\lambda k d) + 2\lambda\mu_{xx} = 0 \tag{25}$$

where $\lambda^2 = -\Lambda^2$ with Λ defined in (24).

Since the surface-type and guided modes occur in the regions $\alpha^2 > 0$ and $\alpha^2 < 0$ respectively the limiting frequencies are the same as those found in the previous section. That is, surface modes occur for $\omega > \omega_c$ and guided modes for $\omega_l < \omega < \omega_c$ with ω_l and ω_c given by (18) and (16) respectively. The critical angle θ_c remains of relevance to the surface-type modes. Now, however, non-reciprocity takes the form of non-reciprocal localization of the mode functions. In a wedge about the positive X axis defined by θ_c there is a surface-type mode with ψ taking large values near the upper surface and small values near the lower surface. A mode is also found in the corresponding wedge about the negative X axis but with localization at the lower surface. This form of non-reciprocity is fully discussed in the standard review [25] on the subject.

Some numerical illustrations for finite depth d are given in figures 4 and 5. As in figure 3, we take the magnetic material as Ni, $4\pi M_0 = 6.032$ kG and we now take the single external-field value $H_0 = 7.032$ kG corresponding to $\omega_0/\omega_m = 1.166$. It follows from (22) that for given H_0 and magnetic fraction f_1 the surface and guided wave frequencies are functions of the direction of propagation θ and the combined wavenumber–depth variable kd. In figure 4 we plot the frequencies as functions of θ with kd as parameter. Comparison of figure 4(a) and (b) and of 4(c) and (d) shows the effect of reducing the magnetic fraction f_1 from 0.8 to 0.4. With a decrease in f_1 the critical angle θ_c increases so the surface mode occupies a smaller wedge about the X axis. We recall, however, that the existence of a surface mode for any value at all of θ is somewhat surprising for $f_1 < 0.5$. The other

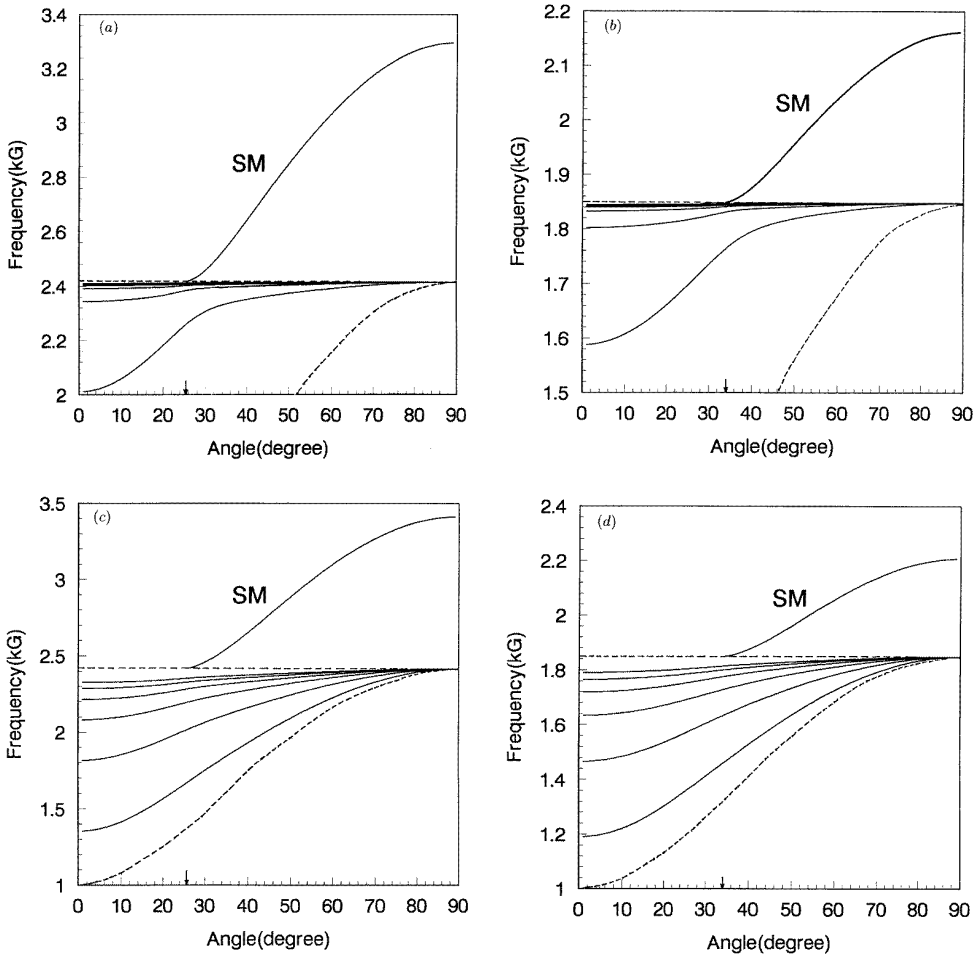

Figure 4. Surface- and guided-mode frequencies versus direction of propagation θ for an LSL of finite depth d. The magnetic material is Ni, $4\pi M_0 = 6.032$ kG and we take external field $H_0 = 7.032$ kG. (a) $kd = 1$, magnetic fraction $f_1 = 0.8$; (b) $kd = 1$, $f_1 = 0.4$; (c) $kd = 5$, $f_1 = 0.8$; (d) $kd = 5$, $f_1 = 0.4$. On each graph we show by an arrow on the θ axis the critical angle θ_c given by (17) and we plot as dashed lines the lower and upper bounds ω_l and ω_c of the guided-wave region. These are given by (18) and (16) respectively.

obvious effect of a decrease in f_1 is that all frequencies decrease, as might be expected when the volume fraction of magnetic material is made smaller. The other comparison, of 4(a) with (c) and of 4(b) with (d), shows the effect of increasing thickness d at fixed magnetic fraction f_1. If d is not too small the surface mode may be regarded as that on the semi-infinite medium perturbed by the boundary condition due to the second surface at $y = -d$. As d increases this perturbation becomes smaller and the surface-mode dispersion curves in figure 4(c) and (d) are closer to those of the semi-infinite LSL (figure 3) than those of figure 4(a) and (b). Formally, the tanh function in (22) or (23) is approaching unity. The other consequence of increasing d is that the intervals between guided-mode dispersion curves become smaller, as is to be expected since they are determined by a standing-wave-type condition.

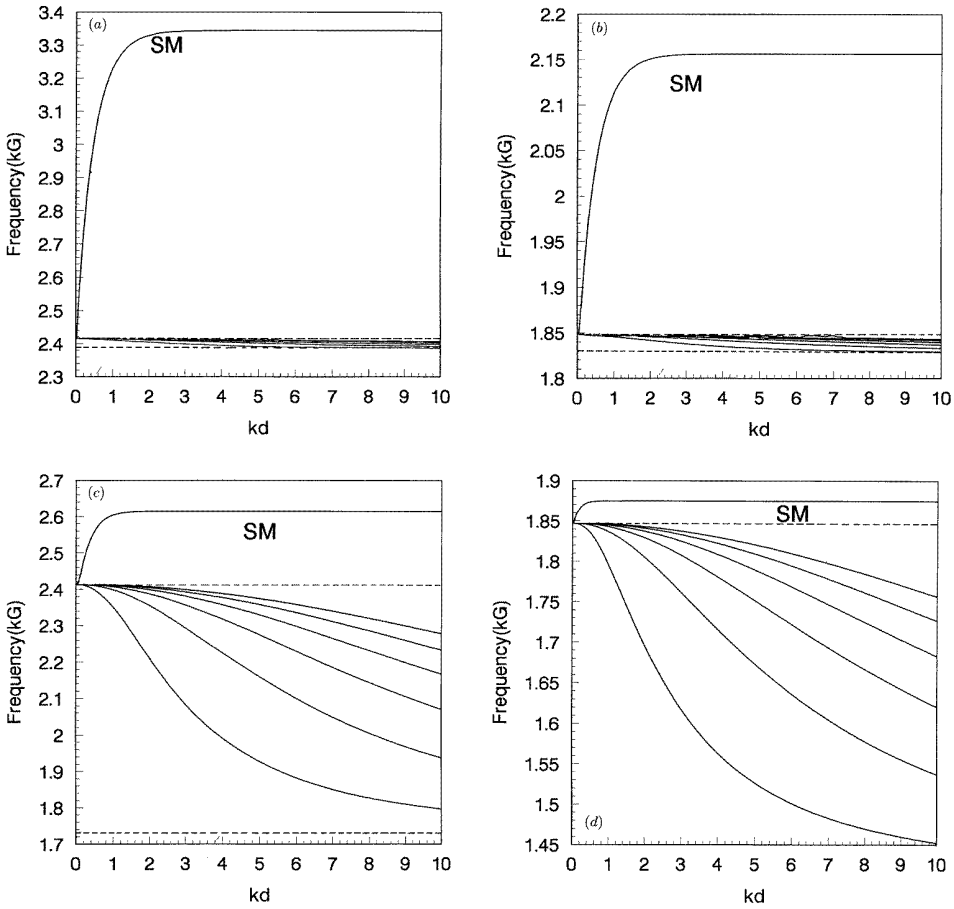

Figure 5. Surface- and guided-mode frequencies versus kd for various θ and f_1. Magnetic parameters as in figure 4. (a) $\theta = 80^\circ$, $f_1 = 0.8$; (b) $\theta = 80^\circ$, $f_1 = 0.4$; (c) $\theta = 40^\circ$, $f_1 = 0.8$; (d) $\theta = 40^\circ$, $f_1 = 0.4$. As in figure 4 the lower and upper bounds θ_l and θ_c of the guided-wave region are shown by dashed lines, except for (d) where $\omega_l = 1.413$ below the scale.

As an alternative, we show in figure 5 mode frequencies versus kd with θ as a parameter. On all the graphs the increase of the surface-mode frequency toward the asymptotic value given by (14) is clear. All four graphs show also a general decrease in the guided-mode frequencies with increasing kd despite the fact that as seen from (16) and (18) and as shown in figure 5(a)–(d) the upper and lower bounding frequencies θ_c and θ_l of the guided-mode region are independent of kd. Comparison of figure 5(a) with (b) and of (c) with (d) shows a general decrease in frequencies and compression of the frequency scales as the magnetic fraction f_1 decreases. Comparison of figure 5(a) with (c) and of 5(b) with (d) shows the effect of decreasing θ, i.e. moving the direction of propagation away from the X axis, for given f_1. The frequency range occupied by the surface mode decreases while that occupied by the guided waves increases.

5. Discussion

Our main results are illustrated in figure 3 for the thick (semi-infinite) LSL and in figures 4 and 5 for the LSL of finite thickness. Qualitatively these have similar properties to the magnetostatic modes of unpatterned films [26]. The surface mode is non-reciprocal, propagating in a wedge of angle $\pi/2-\theta_c$ about the Voigt direction. In figure 3 the surface mode lies above the bulk continuum and in figures 4 and 5 the continuum is replaced by a discrete spectrum of guided modes. The details here depend on the magnetic fraction f_1 and figure 2, for example, shows how θ_c depends on $f_2 = 1-f_1$. One significant difference from most previous work on magnetic superlattices is that we find a surface mode for all values of f_1, whereas in many cases [14–16] the condition $f_1 > 0.5$ is necessary. Another important difference from the earlier work is that there is no simple limit as $f_1 \to 1$ since for any value of f_1 there is a demagnetizing field ensuring that the resonance field is $\omega_i = \omega_0 - \omega_m$, as in (1).

In a magnetostatic mode there is no coupling to the electric field and the present results therefore apply equally to conducting and insulating materials. Clearly it would be of interest to investigate the properties of the retarded (polariton) modes of metallic LSLs in the geometry considered here since the properties of these modes do depend on the E field. For general direction of propagation θ the conductivity may be expected to lead to heavy damping of the polaritons. By analogy with the results of Camley *et al* (18), however, the Voigt direction $\theta = \pi/2$ may be exceptional since this corresponds to the polariton E field lying precisely transverse to the LSL grooves and in this direction the effective conductivity is very small. Thus rapid variation of damping as θ varies around the Voigt direction may be expected.

Acknowledgments

The work of XZW was supported financially by the National Natural Science Foundation of China and the National Natural Science Foundation of Heilongziang Province and DRT was supported by a Short-term Research Grant from Universiti Sains Malaysia. We appreciate helpful discussions with Professor R E Camley.

References

[1] Falicov L M *et al* 1990 *J. Mater. Res.* **5** 1299
[2] Van Roy W, Carpi E L, Van Hove M, Van Esch A, Bogaerts R, De Boeck J and Borghs G 1993 *J. Magn. Magn. Mater.* **121** 197
[3] Ueska Y, Nakatini Y and Hayashi N 1993 *J. Magn. Magn. Mater.* **123** 209
[4] Shearwood C, Ahmed H, Nicholson L M, Bland J A C, Baird M J, Patel M and Hughes H P 1993 *Microelectron. Eng.* **21** 431
[5] Demokritov S and Tsymbal E 1994 *J. Phys.: Condens. Matter* **6** 7145
[6] Dumelow T, Parker T J, Smith S R P and Tilley D R 1993 *Surf. Sci. Rep.* **17** 151
[7] Kamsul Abraha and Tilley D R 1996 *Surf. Sci. Rep.* **24** 125
[8] Wang Xuan-Zhang and Tilley D R 1994 *Phys. Lett.* **187A** 325
[9] Wang Xuan-Zhang and Tilley D R 1994 *Phys. Rev.* B **50** 13 472
[10] Wang Xuan-Zhang and Tilley D R 1995 *Phys. Rev.* B **52** 13 353
[11] Brown D E, Dumelow T, Parker T J, Kamsul Abraha and Tilley D R 1994 *Phys. Rev.* B **49** 12 266
[12] Kamsul Abraha, Brown D E, Dumelow T, Parker T J and Tilley D R 1994 *Phys. Rev.* B **50** 6808
[13] Jensen M R F, Parker T J, Kamsul Abraha and Tilley D R 1995 *Phys. Rev. Lett.* **75** 3756
[14] Camley R E, Rahman T S and Mills D L 1993 *Phys. Rev.* B **27** 261
[15] Grünberg P and Mika K 1993 *Phys. Rev.* B **27** 2955

[16] Almeida N S and Tilley D R 1990 *Solid State Commun.* **73** 23
[17] Liu An-Ting, Wang Xuan-Zhang and Tilley D R 1995 *Phys. Lett.* **199A** 224
[18] Camley R E, Parker T J and Smith S R P 1996 *Phys. Rev.* B **53** 5481
[19] Raj N and Tilley D R 1987 *Phys. Rev.* B **36** 7003
[20] Almeida N S and Mills D L 1988 *Phys. Rev.* B **37** 3400
[21] Agranovich V M and Kravtsov V E 1985 *Solid State Commun.* **55** 373
[22] Raj N and Tilley D R 1985 *Solid State Commun.* **55** 533
[23] Kalinikos B A 1994 *Linear and Nonlinear Spin Waves in Magnetic Films and Superlattices* ed M G Cottam (Singapore: World Scientific) ch 2
[24] Cottam M G and Tilley D R 1989 *Introduction to Surface and Superlattice Excitations* (Cambridge: Cambridge University Press)
[25] Camley R E 1987 *Surf. Sci. Rep.* **7** 103
[26] Damon R W and Eshbach J R 1961 *J. Phys. Chem. Solids* **19** 308